NTU Journal of Engineering and Technology (2025) 4 (1) : 10-23
DOI: https://doi.org/10.56286/ntujet.v4i1

IRAQI Academic Scientific Journals

P-ISSN: 2788-9971 E-ISSN: 2788-998X
NTU Journal of Engineering and Technology
Available online at: https://journals.ntu.edu.iq/index.php/NTU-JET/index

A Technique for Retinal Detachment Detection Manipulating YOLOv8 Models

Younis Bashar Younis[1], Fadwa Al Azzo [2],
[1] Northern Technical University, Technical Engineering College of Mosul, Department of Medical Instrumentation Technology Engineering, Mosul, Iraq, younis.bashar@ntu.edu.iq
[2] Northern Technical University, Technical Engineering College of Mosul, Engineering Department of Cybersecurity Technologies and Cloud Computing, Mosul, Iraq, fadwaalezzo@ntu.edu.iq

Article Informations

Received: 02-06- 2024,
Revised: 29-07-2024,
Accepted: 01-09-2024,
Published online: 22-03-2025

Corresponding author:
Name: Younis B. Younis
Affiliation : Northern Technical University.

Email: younis.bashar@ntu.edu.iq

Key Words:
Retinal Detachment,
Optical Coherence Topography,
YOLOv8,
precision,
recall.

A B S T R A C T

A retinal detachment is a serious condition resulting in the retina detaching from its support layers, which are just beneath it. If untreated, this can cause blindness. To detect the classes of retinal detachment in various images, this paper introduces a novel method employing deep learning techniques involving the YOLOv8 algorithm. Notably, this marks the first use of the YOLOv8 model for retinal detachment detection. Retinal detachment can be identified with high precision using images obtained from Optical Coherence Tomography (OCT). The proposed work assesses the performance of these models using metrics such as mAP50, recall, and precision by training five YOLOv8 models: YOLOv8n, YOLOv8s, YOLOv8m, YOLOv8l, and YOLOv8x. Among these, the YOLOv8s model had the best performance with a mAP50 of 0.985, a recall of 0.97, and a precision of 0.968. The other models had the following mAP scores: YOLOv8n (0.949), YOLOv8m (0.906), YOLOv8l (0.889), and YOLOv8x (0.907). This demonstrates that the proposed system works effectively in detecting retinal detachment, resulting in highly accurate results mined from complex medical data sets and imaging, thereby making it an important tool in medicine.

1. Introduction

An important organ that is necessary for daily human activities is the eye. the major sensory organ for vision is the eyes, which enables humans to interpret information and see the surroundings. The retina is a crucial component of the eye that is vital to vision. The eye is a complicated organ that depends on several vital components to function. The main structures that make up the eye are the cornea, iris, pupil, lens, optic nerve, and retina. The main job of the retina is to convert light from the focal length of the lens into message signals that the brain uses for visual recognition. Consequently, the retina is regarded as an important eye component for identifying different nearby objects[1]. All ages are increasingly experiencing retinal-based disorders, which impair vision clarity by causing fuzzy images and even total blindness[2]. A severe medical disease known as RD causes the retinal layers to separate from their natural position. It's a strict visual trouble that needs to be treated right away to avoid irreversible vision loss. Retinal lesions such as retinal bleeding and retinal holes may result from repeated RD[3]. RD diagnosis made early and accurately is essential for prompt intervention and improved patient results[4]. Even though most instances are asymptomatic in the course of the initial tiers of the disorder, its early detection and treatment can help to postpone or avoid a terrible evolution[5]. When a young patient provides with abrupt unilateral imaginative and prescient loss, there are numerous in all likelihood reasons, such as optic neuropathy or retinopathy[6]. When diagnosing and treating RD, medical imaging is necessary. RD can worsen and cause a substantial loss of vision if treatment is not received. The likelihood of irreversible vision damage increases with the time the retina is detached. Classifying retinal diseases poses a serious challenge to Computer-Aided Diagnosis (CAD) in the medical field. RD is the term used to describe the division of the Neurosensory Retina (NSR) from the underlying retinal pigment epithelium (RPE). When the adhesion forces between the RPE and NSR are too great, an RD happens. This can happen through a variety of mechanisms. Irrespective of the mechanism involved, all forms of RD share a common characteristic, namely the buildup of fluid beneath the retina[7]. Notably, there are several types of retinal detachment. depending on the degree of the detachment or the causes Diabetic macular edema (DME) is characterized by the presence of retinal thickening resulting from the buildup of intraretinal fluid, Most of patients got blindness because of diabetic retinopathy (DR)[8], predominantly within the inner and outer plexiform layers, One element of the exudative Age-related Macular Degeneration is Choroidal Neovascularization (CNV), characterized by the atypical development of blood vessels originating from the choroidal vasculature and extending into the neurosensory retina by traversing the Bruch's membrane and DRUSEN which are small yellow deposits of fatty proteins (lipids) that accumulate under the retina. Typically, there are 12 instances of RD consistent with 100,000 human beings every year[9]. Numerous imaging modalities, including fundus photography, B-scan ultrasonography, and OCT offer comprehensive details on the retinal structure and assist medical professionals in determining the kind and degree of RD. Optical coherence tomography angiography (OCT-A) gives excessive-decision images of retinal anatomy and microvasculature trough some modalities permitting signal penetration to the choroid[10]. The OCT imaging method is similar to ultrasound imaging, although it differs slightly in terms of detection. OCT imaging uses light waves as opposed to sound waves, which record the ultrasound image[11]. The training dataset, which was made up of OCT images, was acquired between July 1, 2013, and March 1, 2017, from the following sources: Beijing Tongren Eye Center, Medical Center Ophthalmology Associates, the Shiley Eye Institute of the University of California San Diego, Shanghai First People's Hospital, and California Retinal Research Foundation[12]. The advent of artificial intelligence (AI) has remarkable promise for tackling many diagnostic and healing demanding situations in medicine[13]. Modern medicine is built on signs that can not be observed by doctors but that can be identified through the application of Deep Learning (DL) and big data approaches, technology of this kind can analyze and comprehend a far greater amount of data than any human could, researchers in the medical and healthcare fields are becoming more and more interested in DL since it can improve the accuracy of medical applications by utilizing medical data[14]. Within pc vision, the YOLO series of algorithms has gained considerable popularity[15]. Within the quickly developing field of computer vision, two technologies RoboFlow and YOLOv8 have become essential for developing effective and precise object detection systems. Roboflow is an online computer vision platform that makes it possible for users to produce robust and rapid computer vision models[16]. Much less effort and time might be required with automated analysis and prognosis[17].

2. Related Work

In 2019, Feng Li et al[18] Images of OCT were automatically analyzed to detect DRUSEN, NORMAL, Diabetic Macular Edema (DME), and choroidal neovascularization (CNV). The ensemble of four classification model instances was employed by the proposed classification algorithm to discern retinal OCT images. Each classification model

instance was constructed using an enhanced Residual Neural Network (ResNet50). The suggested methodology attained a classification accuracy of 0.973, a sensitivity of 0.963, and a specificity of 0.985 at the B-scan level, thereby accomplishing a performance that matches or surpasses that of ophthalmologists possessing ubstantial clinical expertise. A total of 21,357 retinal OCT images were collected from 2,796 adult patients between 2014 and 2019.

In 2020, Timo Kepp *et al*[19] applied the CNN for accurate segmentation of the total retina and Pigment Epithelial Detachment (PED). The U-Net architecture, a popular CNN architecture in biomedical image analysis, was used as the basis for the CNN. The dataset used in the study consists of image data acquired from a group of 51 patients using the OCT system. Each patient had both eyes scanned, resulting in a doubled number of image data. The U-Net approach achieved high accuracy in segmenting the total retina, with a Dice Similarity Coefficient (DSC) of 0.939. However, the segmentation of PEDs proved to be more challenging, with a DSC of 0.593. The Convolutional Denoising Auto Encoder (CDAE) refinement improved the segmentation results, with minimal deviations for both retina and PED. The quantitative evaluation indicated that the retina was segmented with high accuracy.

In 2021, Wang *et al*[20]. proposeded the OCT-DeepLab model for segmenting macular edema in OCT images. This model utilizes the DeepLab framework with atrous spatial pyramid pooling (ASPP) for detecting capabilities and a totally related conditional random area for refining obstacles. Compared to conventional and different techniques, OCT-DeepLab showed advanced overall performance in precision, sensitivity and specificity. The version became examined on a dataset of OCT photos with macular edema and carried out a median AUC of 0.963. This have a look at demonstrates OCT-DeepLab's potential to assist ophthalmologists by using supplying correct and green segmentation of macular edema.

In 2021, Hassan *et al*[1]. presented a framework that uses pre-trained network architectures (AlexNet, ResNet-18, and GoogleNet) for classification to automatically diagnose Central Serous Retinopathy (CSR) from OCT images. It included a preprocessing phase to enhance and filter OCT images and evaluate the performance of multiple pre-trained networks. The dataset used in the paper was the Optical Coherence Tomography Image Database (OCTID), which comprises a total of 309 samples, including 102 OCT images of Central Serous Retinopathy (CSR) and 207 images of normal subjects. Approximately 70% of the dataset was used for training, and the remaining 30% was used for validation. The accuracy obtained as a result of each AlexNet, ResNet18, and GoogleNet is 99.64%, 98.19%, and 96.39% respectively.

In 2023, Raluca Brehar *et al*[21] proposed a hybrid method to find unique biomarkers for age-related macular degeneration (AMD) that blends feature-based image classification with deep learning-based retinal layer segmentation. The AROI dataset, which comprises 1,136 pictures from 24 patients with annotations for biomarkers and retinal layers in patients with AMD symptoms, is the dataset that was employed. The paper focused on the segmentation of biomarkers for AMD from retinal OCT images which are capable of accurately detecting the different layers of the retina and any fluids that may appear in the image. A classification method based on features was employed in cases where the flu-ids are difficult to identify. This approach combines textural characteristics with machine learning, resulting in a 90% accurate classification between the fluids and the retinal layers in which they are located.

3. YOLOv8 Network Architecture

YOLO is a network for recognizing target objects. that is renowned for its blazingly quick computing performance and small model size, the simple design of YOLO's neural network enables it to accurately anticipate an object's position and category inside bounding boxes[22]. Ultralytics, the same company that created YOLOv5, launched YOLOv8 in January 2023, there were five scaled variants offered by YOLOv8: YOLOv8n (nano), YOLOv8s (small), YOLOv8m (medium), YOLOv8l (large), and YOLOv8x (extra-large). YOLOv8 is capable of performing a variety of vision tasks, including tracking, segmentation, pose estimation, object identification, and classification[23]. The average accuracy difference between YOLOv8n and YOLOv8x is sixteen.6%, even as YOLOv8n extensively reduces model complexity by means of a thing of 30[24]. The YOLOv8 network typically divides the image into fixed-size grids and uses the information from each grid to identify objects[25]. The input, neck, head, and backbone make up the YOLOv8 network, adaptive anchor box computation, mosaic augmentation, and obtaining picture data to forward it to the subsequent network layer are the main tasks performed at the input stage, the YOLOv8 network typically uses the information from each fixed-sized grid that it creates to recognise objects in the image, as the hub of the network, the backbone is in charge of converting input images into feature maps that incorporate both feature and object positions, In order to collect data from various abstraction levels in the image, the backbone network typically consists of convolutional layers, pooling layers, and further deep learning layers, to improve the gradient flow of the model and fortify the network's feature

Table 1. Models of YOLOv8

Model	size (pixels)	mAP^{val} 50-95	Speed CPU ONNX (ms)	Speed A100 TensorRT (ms)	params (M)	FLOPs (B)
YOLOv8n	640	37.3	80.4	0.99	3.2	8.7
YOLOv8s	640	44.9	128.4	1.20	11.2	28.6
YOLOv8m	640	50.2	234.7	1.83	25.9	78.9
YOLOv8l	640	52.9	375.2	2.39	43.7	165.2
YOLOv8x	640	53.9	479.1	3.53	68.2	257.8

representation. The backbone network's features are further extracted and integrated using the neck layer, The head layer serves as the network's output component and is responsible for Generating object detection results [25]. The Path Aggregation Network (PANet) topology is used by the neck layer of YOLOv8, improving the network's capacity to aggregate object characteristics at different sizes[25]. Figure 1 below shows the architecture of the YOLOv8 network structure.

Table 1 below illustrates the five models that the YOLOv8 algorithm has successfully created. These models are YOLOv8n(nano), YOLOv8s(small), YOLOv8m(medium), YOLOv8l(large), and YOLOv8x(extra-large). and they all have different levels of sub-module depths and widths.

A progressive improvement in the size and precision of the model's detection has been made. Thorough assessment of various YOLOv8 models, examining important metrics like input size (in pixels), meanaverage precision (mAP) at IoU thresholds between 50% and 95%, CPU inference speed using ONNX runtime, GPU inference speed using TensorRT on an NVIDIA A100, model complexity expressed in terms of millions of parameters, and computational complexity expressed in terms of billions of floating-point operations. Together, these measures provide information on the effectiveness, efficiency, and computational needs of the YOLOv8 models.

4. Proposed System

This work aims to present the Retinal Detachment Detection (RDD) system by using YOLOv8 models of deep learning techniques to detect and recognize RD types. The five YOLOv8 models (YOLOV8n, YOLOV8m, YOLOV8s, YOLOV8l, and OLOV8x) are used for this task. The evaluation results of the proposed RDD system are based on the training of RD datasets for four classes. The dataset is preprocessed, which involves applying augmentations and resizing images to speed up network training by utilizing Colab.

The rating of the five models is based on their performance, accuracy, and speed, leading to selecting which is suitable for RD detection. Augments are different image processing methods that are applied to the dataset by Roboflow to produce different versions of the original photos. These modifications improve generalization, robustness of the model, and diversity of datasets. The dataset starts with 419 images and grows to 998 images in total after augmentations. To fit into 640 × 640 pixels, the Augmentation process. An annotation process entails RD image tagging. Figure 2 below shows the proposed system with the training process.

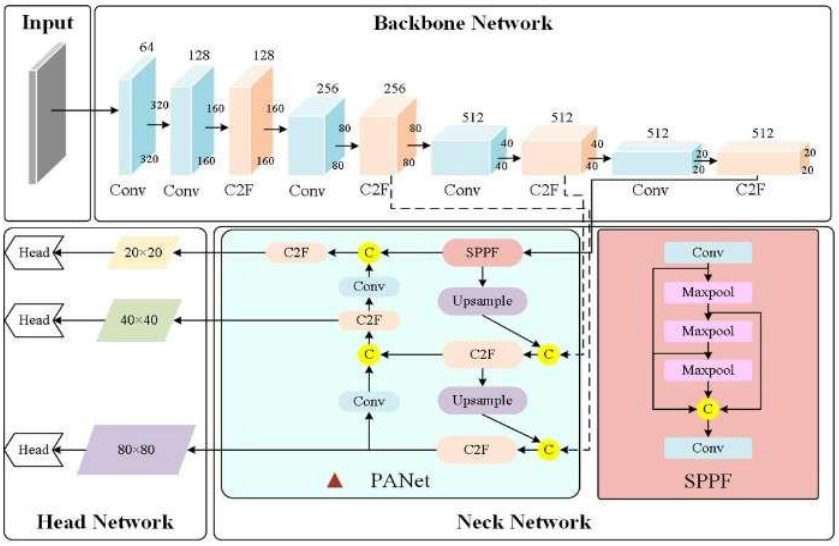

Figure 1. YOLOv8 network structure diagram [14]

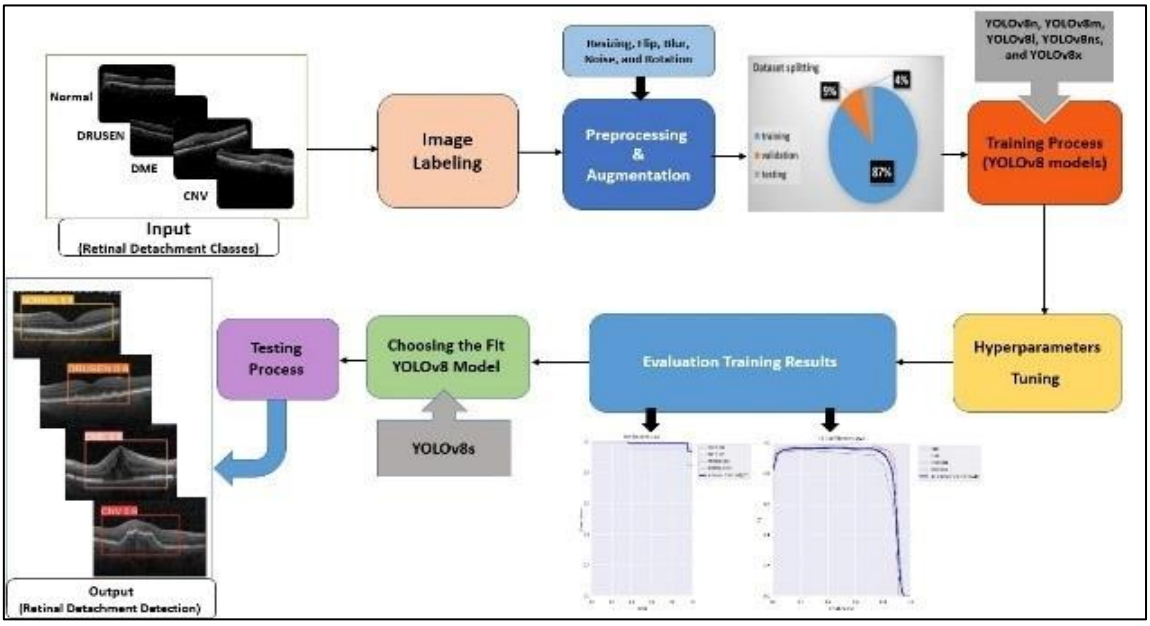

Figure 2. Block diagram of the proposed RDD system

5. Dataset

The dataset utilized in this work, which includes 419 images for four classes (CNV, DME, DRUSEN, and NORMAL), was downloaded from Shiley Eye Institute of the University of California San Diego, the California Retinal Research Foundation, Medical Center Ophthalmology Associates, the Shanghai First People's Hospital, and Beijing Tongren Eye Center[12]. As seen in Figure 3 samples for four classes of the RD dataset. the image was resized. Random rotation between a -15 to +15 degree range was part of the image Augmentation process. An annotation process entails RD image tagging. Figure 3 below presents examples of RD used in the dataset.

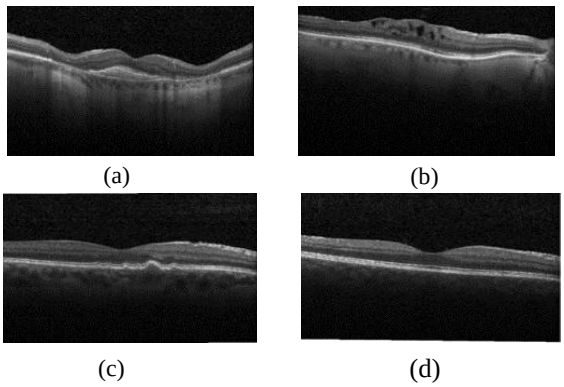

(a) (b) (c) (d)

Figure 3. Samples for four classes of the RD dataset. (a) Choroidal neovascularisation (CNV), (b) Diabetic macular edema (DME), (c) DRUSEN and (d) Normal case

Roboflow provides a splitting dataset into three sections: training, validation, and testing. The splitting percentages for the dataset are as follows. 87% were utilized for training, 8% for validation, and 4% for testing, as Figure 4 below illustrates.

6. Training YOLOv8 models

This section describes the outcomes of the training process for five YOLOV8 models (YOLOV8n, YOLOV8m, YOLOV8s, YOLOV8l, and YOLOV8x) in the Google Colab training environment with an epoch of 100 and a batch size of 16 of each training process. The performance of various models will be compared to determine which produces the best outcomes. In fine-tuning, hyperparameters are adjusted in custom datasets as follows:

- Optimizer: SGD
- Learning rate: 0.01
- Batch size: 16
- Epochs=100

To improve the performance of the YOLOv8 model, a thorough fine-tuning procedure was carried out, with particular attention to data distribution for training, validation, and testing. Throughout this process, the percentage composition of the dataset allocated to each phase was purposefully changed. The data distribution was carefully experimented with and modified repeatedly to maximize the model's capacity for generalization and improve its forecast accuracy.

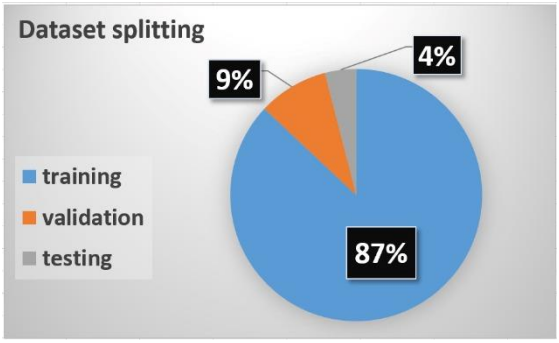

Figure 4. Splitting Percentages for the Dataset

Use a single command to install all dependencies and needs for YOLOv8 models (! pip install ultralytics==8.0.20). Models need to be connected to a T4 GPU inside Google Colab before training, as illustrated in Figure 5 below

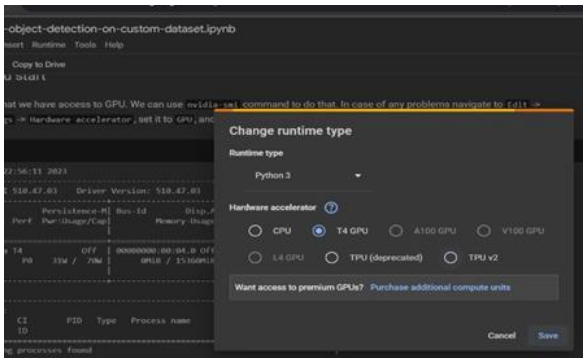

Figure 5. Choosing the Access to GPU

Access to GPU or not, as shown in Figure 6 below, by using the following command on Google Colab (! nvidia-sm).

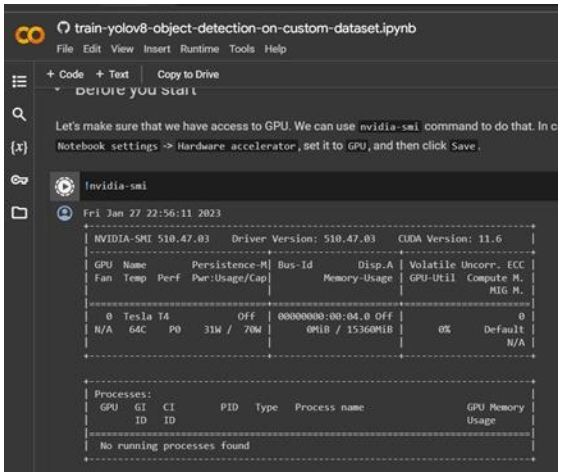

Figure 6. Show the Access to GPU

Execute the subsequent instruction, by running the the code
(!yolo task=detect mode=train model=yolov8s.pt data={dataset. location}/
data.yaml epochs=100 imgsz=640 plots=True), to select one of the expanded models. The formula for train mode is
mode = train.
Task = detect
model = the detection model, and
epochs = the number of epochs used to train the model is how detection is expressed. After downloading the model and image, it will forecast the corresponding image. Once the training process is finished, the train folder has several files, including charts, the Confusion Matrix, the precision-recall curve, weights, and so on. By right-clicking on the best file and selecting download, as illustrated in Figure 7, you can save the weights of the trained model in a file format with the pt extension.

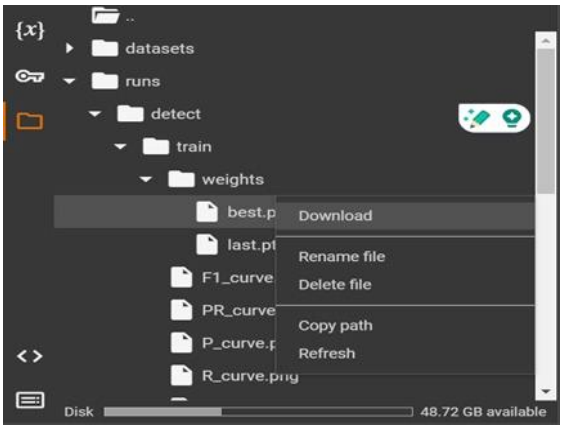

Figure 7. Storing the Trained Model's Weights in Storage

7. Results and Discussion

This section illustrates the results and testing results of the five models of YOLOv8 separately. The results are shown for each model independently, along with a comparison table comparing all of the models and a relationship chart showing the relationship between precision and recall curve and confidence and precision. Using all five of the YOLOv8 models YOLOv8n, YOLOv8m, YOLOv8s, YOLOv8l, and YOLOv8x comprising the four classes (CNV, DME, DRUSEN, and NORMAL) were trained. Achieving high precision and recall during YOLOv8 model training is crucial for the overall performance of the model. For every class, the Average Precision (AP) is obtainedRecall measures the proportion of actual positive instances that are correctly identified by a model among all the positive instances. The AP is then averaged over multiple courses to determine the mAP. Precision is defined as the ratio of correctly classified positive replies (true positives) to the total number of incorrectly classified but positively labelled replies (false positives)[27]. For the validation process, the impact of the number of epochs on mAP@0.5 and mAP@0.5_0.95 is significant. The training results for the YOLOV8 models demonstrate a consistent decline in the overall loss value of the validation processes. Figure 7 shows the Losses of Training and Validation following each training session. The x-axis represents the epoch number, while the y-axis indicates box_loss, obj_loss, and cls_loss, respectively. The terms train/box_loss and val/box_loss refer to bounding box loss in training and validation procedures. Reducing bounding box loss results in more accurate results. Train/obj_loss and val/obj_loss represent the average losses for object detection in training and validation runs, respectively, and lower loss targets lead to more accurate detection. Train/cls_loss and val/cls_loss

indicate the average classification loss during training or validation procedures, and a smaller classification loss results in a more accurate classification. for the other evaluation metrics (mAP-50,mAP-95, and precision) the x-axis represents the number of epochs while the y-axis is the mean average precision-50, Recall, and precision, as shown in figure 8 below.

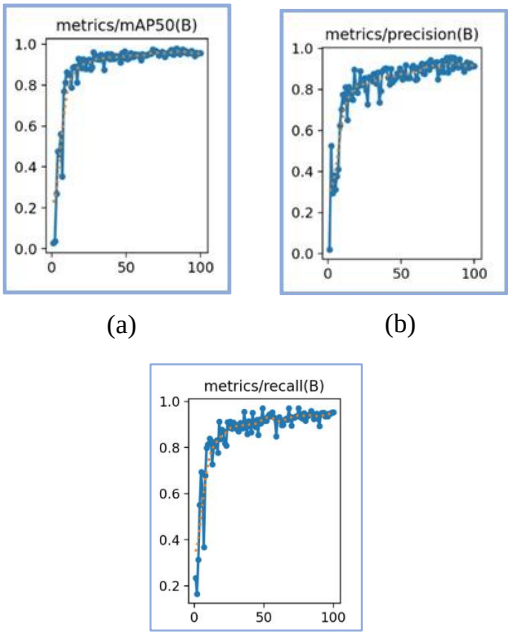

(a) (b)

(c)

Figure 8. Metrics' outcomes in the YOLOv8 models' training process (a) mAP50, (b) Precision, and (c) Recall

7.1 Training result of YOLOv8s

Achieving high precision and recall during YOLOv8 model training is crucial for the overall performance of the model. The superior performance of the YOLOV8s model on training data is compared to other YOLOV8 models, such as YOLOV8l, YOLOV8m, YOLOV8n, and YOLOV8x. After 100 epochs, the YOLOv8s model produces a recall of 0.97, a mAP50 of 0.985, precision of 0.968. Figure 9 below shows the results of metrics in the training progress of retinal detachment detection. The most important assessment metric is mAP50, which gauges the model's precision in object detection and localization inside an image as opposed to its categorization performance. After determining the average precision for each class, it computes the mean across all classes. The mAP50 value of YOLOv8s was 0.985, suggesting enhanced object detection throughout the dataset studied.

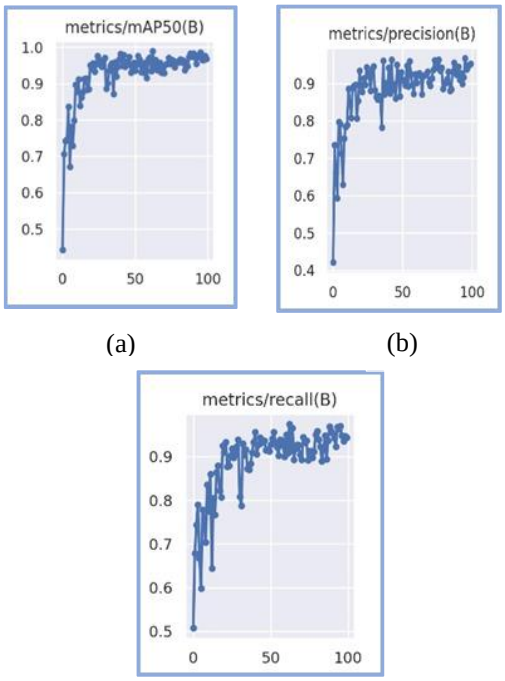

(a) (b)

(c)

Figure 9. Metrics' outcomes in the YOLOv8s model's training process (a) mAP50, (b) Precision, and (c) Recall

Smaller loss targets which begin with a large value and go smaller and smaller achieve more accurate detection. The lowest amount of losses was achieved by YOLOv8s in contrast to other YOLOv8 models, this is seen in Figure 10 below.

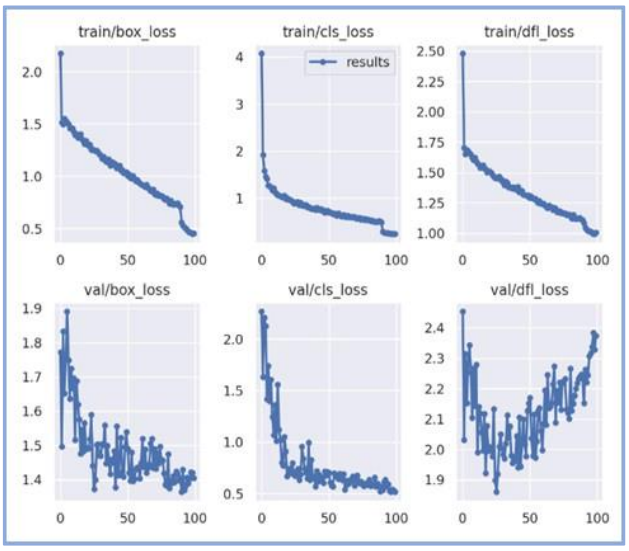

Figure 10. The losses of training and validation results of YOLOv8s

7.2 Training result of YOLOv8n

After 100 epochs, the YOLOv8n model achieves a precision score of 0.949, a recall score of 0.963, and a mean Average Precision at 50% intersection over union (mAP50) of 0.977 for detecting retinal detachment. Figure 11 illustrates the training progress and the corresponding metrics.

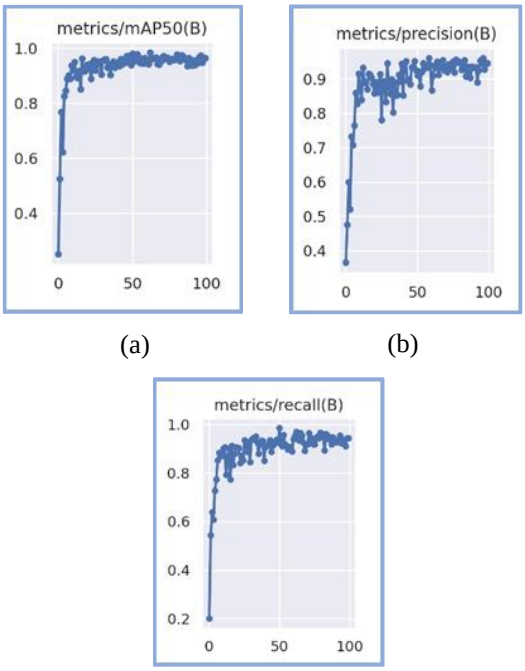

Figure 11. Metrics' outcomes in the YOLOv8n model's training process (a) mAP50, (b) Precision, and (c) Recall

The results of losses in training and validation progress for YOLOv8n are shown in Figure 12 below.

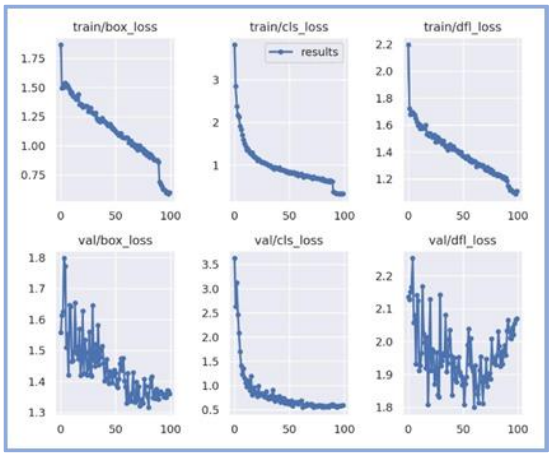

Figure 12. YOLOv8n's Results of losses in training and validation progress

7.3 Training result of YOLOv8m

After 100 epochs, the YOLOv8m model produces a precision of 0.906, recall of 0.975, and mAP50 of 0.974. The metrics used in the training process of retinal detachment detection are displayed in Figure 13 below.

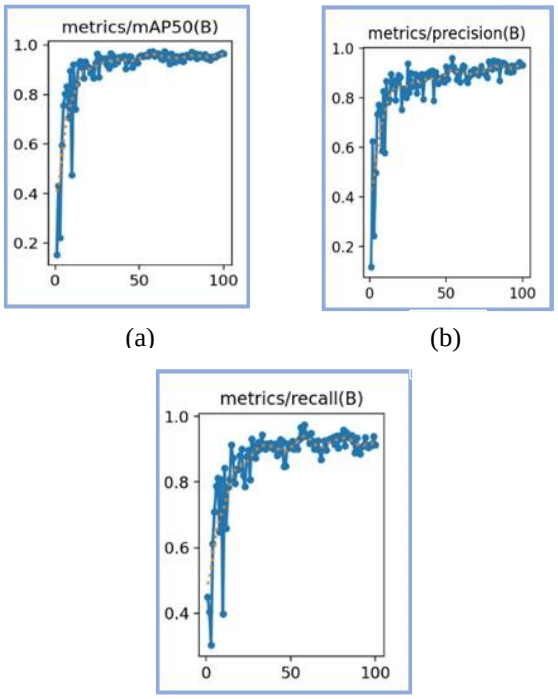

Figure 13. Metrics' outcomes in the YOLOv8m model's training process (a) mAP50, (b) Precision, and (c) Recall

Results of losses in training and validation progress for YOLOv8m are shown in Figure 14 below.

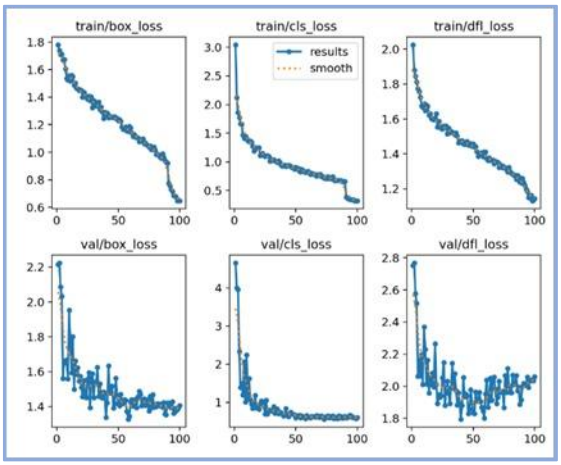

Figure 14. YOLOv8m's Results of losses in training and validation progress

7.4 Training result of YOLOv8l

YOLOv8l model yields a precision of 0.889, recall of 0.892, and mAP50 of 0.934 after 100 epochs. Figure 15 below shows the results of metrics in the training progress of retinal detachment detection.

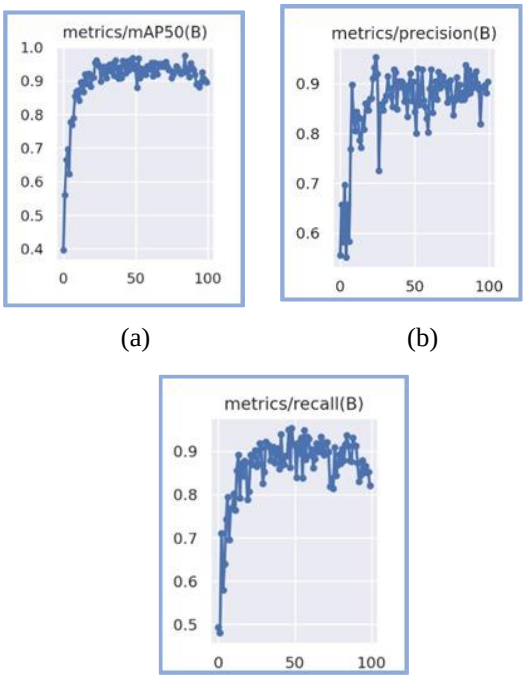

Figure 15. Metrics' outcomes in the YOLOv8l model's training process (a) mAP50, (b) Precision, and (c) Recall

The results of losses in training and validation progress for YOLOv8l are shown in Figure 16 below.

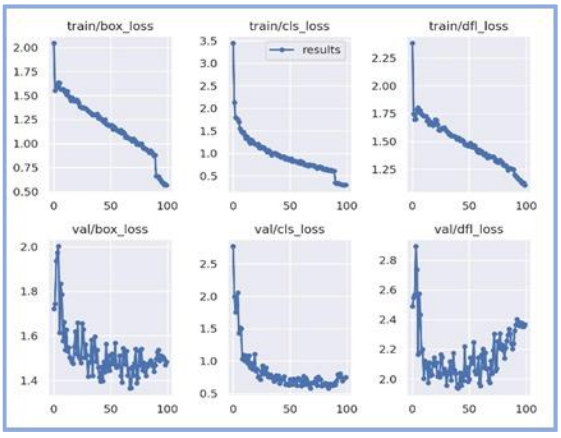

Figure 16. YOLOv8l's Results of losses in training and validation progress

7.5 Training result of YOLOv8x

YOLOv8x model yields a precision of 0.907, recall of 0.916, and mAP50 of 0.947 after 100 epochs. Figure 17 below shows the results of metrics in the training progress of retinal detachment detection.

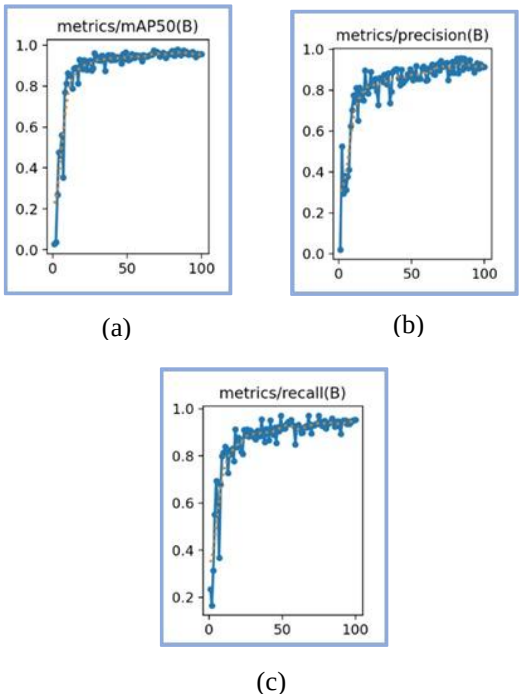

Figure 17. Metrics' outcomes in the YOLOv8x model's training process (a) mAP50, (b) Precision, and (c) Recall

The results of losses in training and validation progress for YOLOv8x are shown in Figure 18 below.

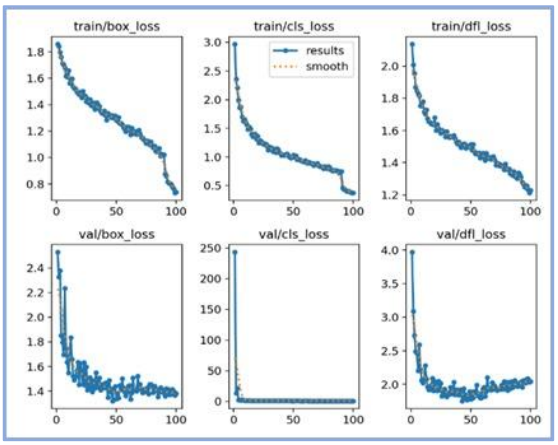

Figure 18. YOLOv8x's Results of losses in training and validation progress

7.6 Comparison of YOLOv8 models' performance evaluation for RDD system

The training executed to other models with the same hyperparameter to additional YOLOv8 models

(YOLOv8n, YOLOv8m, YOLOv8l, YOLOv8s, and YOLOv8x) to see which model performs better based on assessment metrics like mAP50, Recall, and Precision. the YOLOV8s model performs better on training data than the YOLOV8l, YOLOV8m, YOLOV8n, and YOLOV8x models. After 100 epochs, the YOLOV8s model produces results with a precision of 0.968, recall of 0.97, and mAP50 of 0.985. The comparison of the results of five YOLOV8 models is summarised in Table2.

7.7 Testing results

In this study, we evaluated the performance of YOLOv8 models in retinal detachment disease models. Models tested include YOLOv8s, YOLOv8n, YOLOv8m, YOLOv8l and YOLOv8x. Each model was evaluated for its ability to accurately recognize and classify images in NORMAL, DME, DRUSEN, and CNV classes. Below, we provide an assessment of the performance of each model, highlighting their strengths and weaknesses.

7.7.1 YOLOv8s testing result

The YOLOv8s model demonstrated the highest detection accuracy among the tested models. It effectively identified retinal detachment disease images with a high degree of confidence, making it the most efficacious model in this study, see Figure 18 for YOLOv8s results.

Table 2. Performance comparison of the RDD system with five models of YOLOv8

Model	Precision	Recall	mAP50
YOLOv8s	**0.968**	**0.97**	**0.985**
YOLOv8n	0.949	0.963	0.977
YOLOv8m	0.906	0.975	0.974
YOLOv8l	0.889	0.892	0.934
YOLOv8x	0.907	0.916	0.947

7.7.2 YOLOv8n testing result

The YOLOv8n model showed strong detection abilties. While its overall performance changed into slightly decrease than YOLOv8s, it turned into still powerful in detecting retinal detachment diseases ,see Figure19 for YOLOv8n result

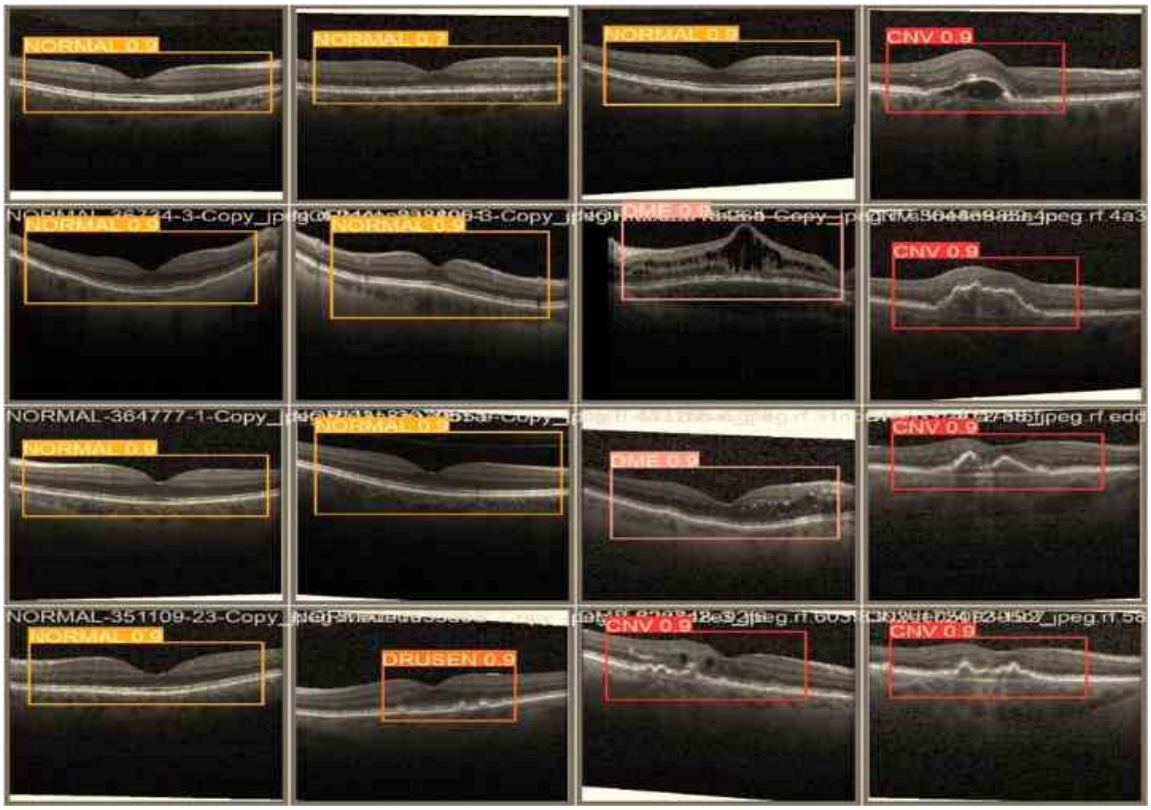

Figure 19. YOLOv8s Testing results in the bounded box with the confidence score for four classes of retinal detachment disease detection (Normal, DME, DRUSEN, and CNV)

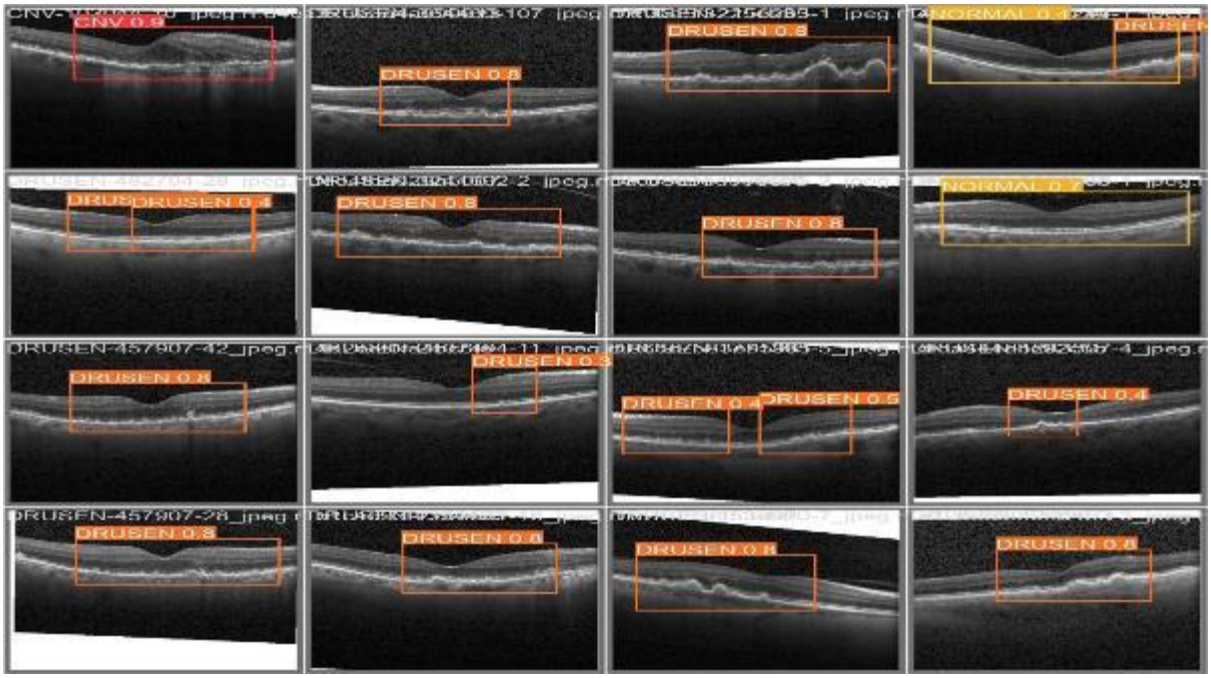

Figure 20. YOLOv8m Testing results in the bounded box with the confidence score for four classes of retinal detachment disease detection (Normal, DME, DRUSEN, and CNV)

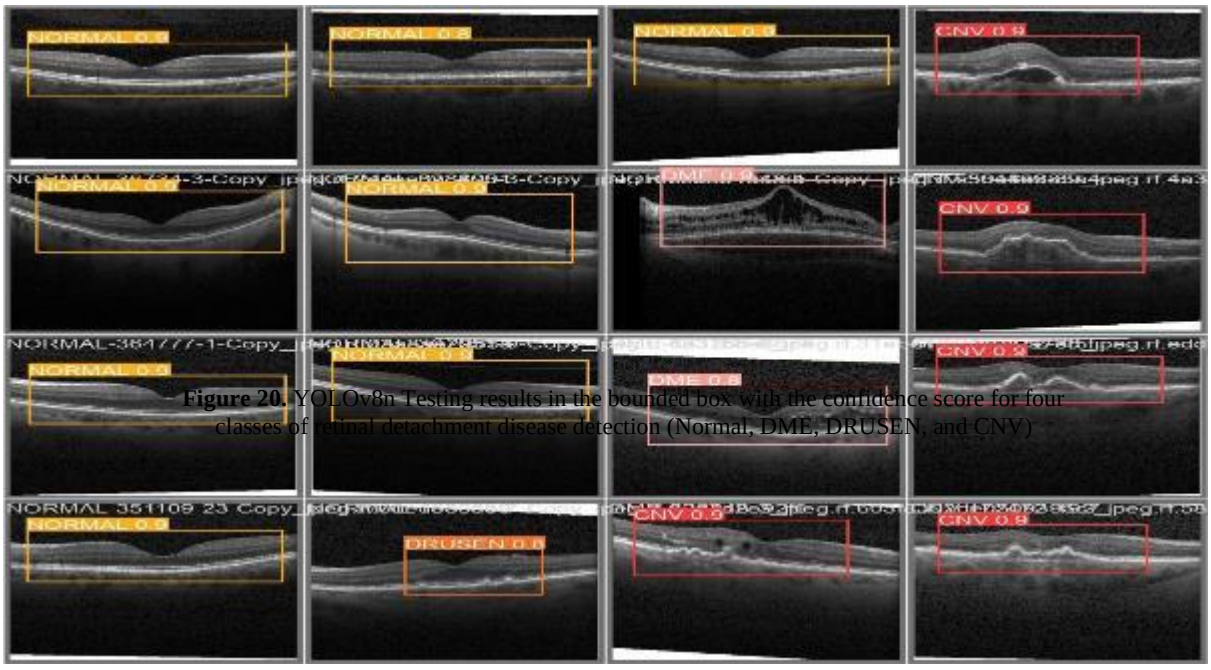

Figure 20. YOLOv8n Testing results in the bounded box with the confidence score for four classes of retinal detachment disease detection (Normal, DME, DRUSEN, and CNV)

Figure 21. YOLOv8l Testing results in the bounded box with the confidence score for four classes of retinal detachment disease detection (Normal, DME, DRUSEN, and CNV)

7.7.3 YOLOv8m testing result

The YOLOv8m version exhibited true detection accuracy. Its overall performance became akin to YOLOv8n, although it did now not outperform the YOLOv8s version, see Figure 20 for YOLOv8m outcomes.

7.7.4 YOLOv8l testing result

The YOLOv8l model accomplished reasonably well. It confirmed affordable detection accuracy but did not suit the overall performance of the YOLOv8s, YOLOv8n, and YOLOv8m fashions, see Figure 21 for YOLOv8l result.

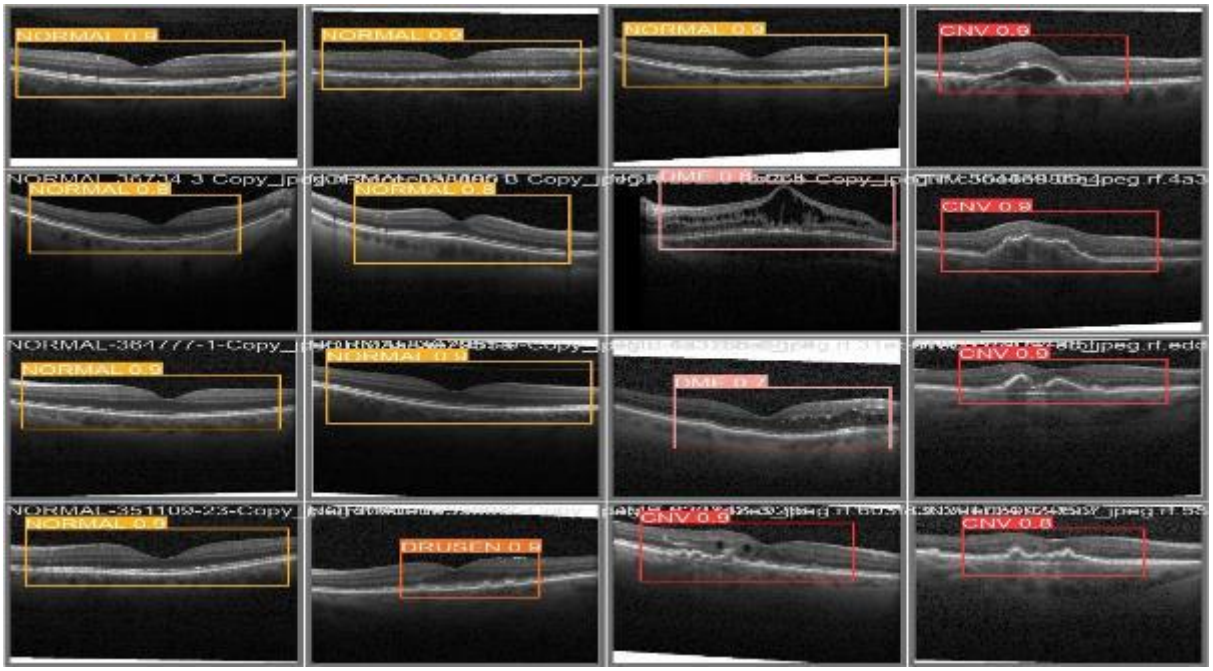

7.7.5 YOLOv8x testing result

The YOLOv8x model had sturdy detection abilities. While its performance was stable, it did not gain the equal stage of accuracy as the YOLOv8s model, see Figure 22 for YOLOv8x outcomes.

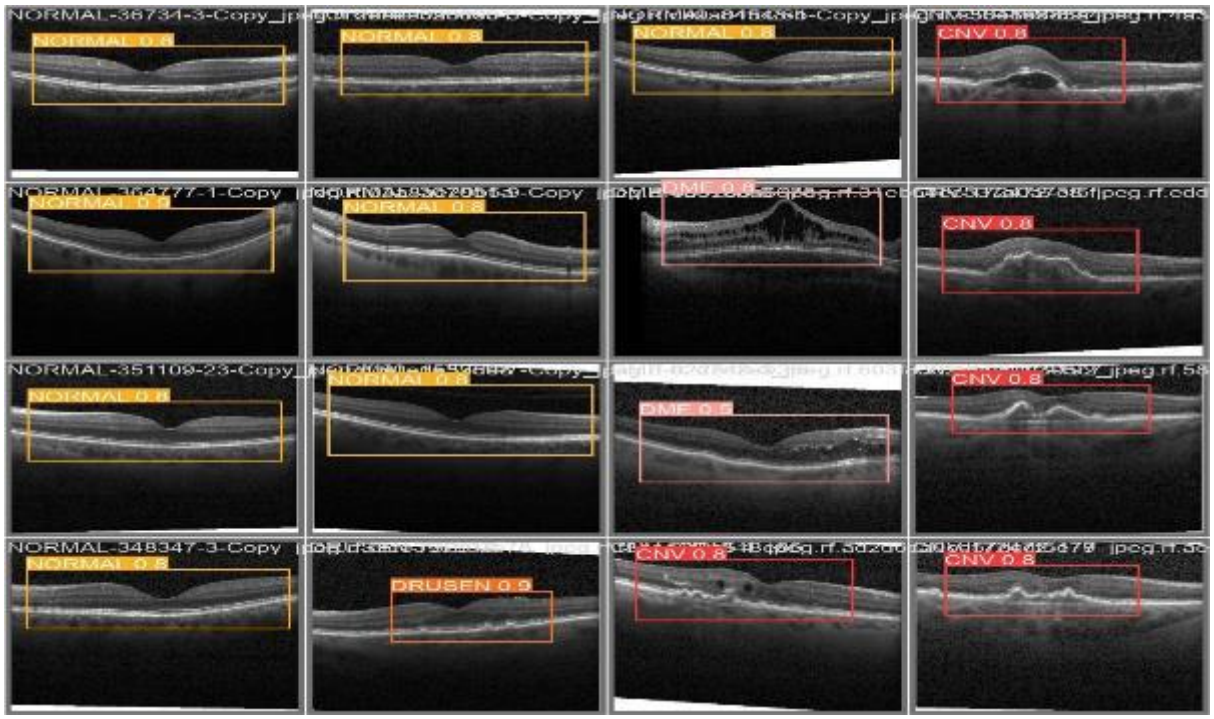

8. Conclusion

In conclusion, the proposed RDD system for retinal detachment disease detection, covering NORMAL, DME, DRUSEN, and CNV classes, is based on the YOLOv8 algorithm, marking the first use of YOLOv8 for this purpose. Various YOLOv8 models—YOLOv8n, YOLOv8s, YOLOv8m, YOLOv8l, and YOLOv8x—were trained and compared. Among these, the YOLOv8s model achieved the best performance with a precision of 0.968, recall of 0.97, and mAP50 of 0.985 after 100 epochs. Precision measures the accuracy of positive predictions, recall assesses the model's ability to identify all relevant instances, and mAP50 is the mean Average Precision at 50% intersection over union, reflecting overall performance. The comparative study highlighted YOLOv8s as not only the most accurate but also the most computationally efficient model. This demonstrates the strong capability of YOLOv8s in recognizing retinal detachment diseases, confirming its suitability for medical applications and establishing its novelty in the field.

REFERENCES

[1] S. A. E. Hassan, S. Akbar, S. Gull, A. Rehman, and H. Alaska, "Deep Learning-Based Automatic Detection of Central Serous Retinopathy using Optical Coherence Tomographic Images," *2021 1st Int. Conf. Artif. Intell. Data Anal. CAIDA 2021*, pp. 206–211, 2021, doi: 10.1109/CAIDA51941.2021.9425161.

[2] R. F. Mullins, S. R. Russell, D. H. Anderson, and G. S. Hageman, "Drusen associated with aging and age-related macular degeneration contain proteins common to extracellular deposits associated with atherosclerosis, elastosis, amyloidosis, and dense deposit disease," *FASEB J.*, vol. 14, no. 7, pp. 835–846, 2000, doi: 10.1096/fasebj.14.7.835.

[3] W.-D. Zhou, L. Dong, K. Zhang, Q. Wang, L. Shao, Q. Yang, Y.-M. Liu, L.-J. Fang, X.-H. Shi, C. Zhang, R.-H. Zhang, H.-Y. Li, H.-T. Wu, and W.-B. Wei, "Deep Learning for Automatic Detection of Recurrent Retinal Detachment after Surgery Using Ultra-Widefield Fundus Images: A Single-Center Study," *Adv. Intell. Syst.*, vol. 4, no. 9, pp. 1–8, 2022, doi: 10.1002/aisy.202200067.

[4] M. Iida, H. Horiguchi, S. Katagiri, Y. Shirakashi, Y. Yamada, H. Gunji, and T. Nakano, "Association of meteorological factors with the frequency of primary rhegmatogenous retinal detachment in Japan," *Sci. Rep.*, vol. 11, no. 1, pp. 1–7, 2021, doi: 10.1038/s41598-021-88979-x.

[5] E. Parra-Mora, A. Cazanas-Gordon, R. Proenca, and L. A. Da Silva Cruz, "Epiretinal membrane detection in optical coherence tomography retinal images using deep learning," *IEEE Access*, vol. 9, pp. 99201–99219, 2021, doi: 10.1109/ACCESS.2021.3095655.

[6] A. G. Lee, "How to distinguish retinal disorders from causes of optic nerve dysfunction ?".

[7] N. G. Ghazi and W. R. Green, "Pathology and pathogenesis of retinal detachment," *Eye*, vol. 16, no. 4, pp. 411–421, 2002, doi: 10.1038/sj.eye.6700197.

[8] J. Lachure, A. V. Deorankar, S. Lachure, S. Gupta, and R. Jadhav, "Diabetic Retinopathy using morphological operations and machine learning," *Souvenir 2015 IEEE Int. Adv. Comput. Conf. IACC 2015*, pp. 617–622, 2015, doi: 10.1109/IADCC.2015.7154781.

[9] M. Colucciello, "Rhegmatogenous retinal detachment," *Phys. Sportsmed.*, vol. 37, no. 2, pp. 59–65, 2009, doi: 10.3810/psm.2009.06.1710.

[10] J. D. Arias, M. M. Parra, A. T. Hoyos, F. Arango, E. J. Viteri, and J. F. Arevalo, "En face swept-source optical coherence tomography angiography choroidal vasculography (CVG) a tool to discriminate choroidal abnormalities in polypoidal choroidal vasculopathy," *Expert Rev. Med. Devices*, vol. 18, no. 9, pp. 903–908, 2021, doi: 10.1080/17434440.2021.1963230.

[11] J. Amin, M. Sharif, A. Rehman, M. Raza, and M. R. Mufti, "Diabetic retinopathy detection and classification using hybrid feature set," *Microsc. Res. Tech.*, vol. 81, no. 9, pp. 990–996, 2018, doi: 10.1002/jemt.23063.

[12] "New Text Document (5)." 1390. [Online]. Available: https://www.kaggle.com/datasets/paultimothymooney/kermany2018/code

[13] S. J. Thomas, M. L'Azou, A. D. T. Barrett, and N. A. C. Jackson, "Fast-Track Zika Vaccine Development — Is It Possible?," *N. Engl. J. Med.*, vol. 375, no. 13, pp. 1212–1216, 2016, doi: 10.1056/nejmp1609300.

[14] F. Piccialli, V. Di Somma, F. Giampaolo, S. Cuomo, and G. Fortino, "A survey on deep learning in medicine: Why, how and when?," *Inf. Fusion*, vol. 66, no. July 2020, pp. 111–137, 2021, doi: 10.1016/j.inffus.2020.09.006.

[15] F. M. Talaat and H. ZainEldin, "An improved fire detection approach based on YOLO-v8 for smart cities," *Neural Comput. Appl.*, vol. 35, no. 28, pp. 20939–20954, 2023, doi: 10.1007/s00521-023-08809-1.

[16] N. Panteleimon, "Propulsion Shafting Arrangement Modeling from Mechanical Drawings using Deep Learning and YOLOv8 DIPLOMA THESIS," no. March, 2023, [Online]. Available: https://dspace.lib.ntua.gr/xmlui/bitstream/handle/123456789/57815/Naoum Panteleimon - Diploma Thesis.pdf?sequence=1

[17] J. Nayak, P. S. Bhat, R. Acharya U, C. M. Lim, and M. Kagathi, "Automated identification of diabetic retinopathy stages using digital fundus images," *J. Med. Syst.*, vol. 32, no. 2, pp. 107–115, 2008, doi: 10.1007/s10916-007-9113-9.

[18] F. Li, H. Chen, Z. Liu, X. Zhang, M. Jiang, Z. Wu, and K. Zhou, "Deep learning-based automated detection of retinal diseases using optical coherence tomography images," *Biomed. Opt. Express*, vol. 10, no. 12, p. 6204, 2019, doi: 10.1364/boe.10.006204.

[19] T. Kepp, H. Sudkamp, C. von der Burchard, H. Schenke, P. Koch, G. Hüttmann, J. Roider, M. P. Heinrich, and H. Handels, "Segmentation of retinal low-cost optical coherence tomography images using deep learning," no. March 2020, p. 56, 2020, doi: 10.1117/12.2551324.

[20] Z. Wang, Y. Zhong, M. Yao, Y. Ma, W. Zhang, C. Li, Z. Tao, Q. Jiang, and B. Yan, "Automated segmentation of macular edema for the diagnosis of ocular disease using deep learning method," *Sci. Rep.*, vol. 11, no. 1, pp. 1–12, 2021, doi: 10.1038/s41598-021-92458-8.

[21] R. Brehar, A. Groza, I. Damian, G. Muntean, and S. D. Nicoara, "Age-Related Macular Degeneration Biomarker Segmentation from OCT images," *Proc. - 2023 24th Int. Conf. Control Syst. Comput. Sci. CSCS 2023*, no. August, pp. 444–451, 2023, doi: 10.1109/CSCS59211.2023.00076.

[22] H. Salim and Fadwa S. Mustafa, "A COMPREHENSIVE EVALUATION OF YOLOv5s AND YOLOv5m FOR DOCUMENT LAYOUT ANALYSIS," no. January, pp. 284–289, 2023.

[23] "Contributors, M. YOLOv8 by MMYOLO. 2023. Available online: https://github.com/open-mmlab/mmyolo/tree/main/ configs/yolov8 (accessed on 13 May 2023).," vol. 8, no. May, p. 2023, 2023.

[24] L. Alzubaidi, J. Zhang, A. J. Humaidi, A. Al-Dujaili, Y. Duan, O. Al-Shamma, J. Santamaría, M. A. Fadhel, M. Al-Amidie, and L. Farhan, *Review of deep learning: concepts, CNN architectures, challenges, applications, future directions*, vol. 8, no. 1. Springer International Publishing, 2021. doi: 10.1186/s40537-021-00444-8.

[25] B. Luo, Z. Kou, C. Han, and J. Wu, "A 'Hardware-Friendly' Foreign Object Identification Method for Belt Conveyors Based on Improved YOLOv8," *Appl. Sci.*, vol. 13, no. 20, p. 11464, 2023, doi: 10.3390/app132011464.

[26] "Ultralytics. YOLOv8 — Ultralytics YOLOv8 Documentation. 2023. Available online: https://docs.ultralytics.com/models/yolov8/ (accessed on 20 November 2023).," no. November, p. 2023, 2023.

[27] A. S. T. Gona Mohammed,Fadwa S. Mustafa, "Real-Time Human Detection and Tracking Based on Deep Learning Technique for Social Distance," no. February, 2023.